Citation
Li, H. and Chen, W. and Pham, T.M. and Hao, H. 2021. Analytical and numerical studies on impact force profile of RC beam under drop weight impact. International Journal of Impact Engineering. 147: ARTN 103743.
http://doi.org/10.1016/j.ijimpeng.2020.103743

Analytical and numerical studies on impact force profile of RC beam under drop weight impact

Huawei Li, Wensu Chen*, Thong M. Pham, Hong Hao*

Center for Infrastructural Monitoring and Protection, School of Civil and Mechanical Engineering, Curtin University, Australia

* Corresponding authors: wensu.chen@curtin.edu.au (Wensu Chen), hong.hao@curtin.edu.au (Hong Hao)

Abstract: Impact force and structural response of reinforced concrete (RC) beams under drop weight impact have been intensively studied and reported in the literature. The prediction of the peak impact force has been well investigated while the study of the overall impact force profile governing the structural response is limited. The impact force parameters acting on a structure including the peak impact force, plateau force, and impact duration all affect the structural responses. This study investigates the impact force profiles from drop weight impact on RC beams. The effects of global stiffness (by changing the beam span and boundary condition) on the impact force profile are numerically studied by using LS-DYNA. A two-degree-of-freedom (2DOF) analytical model is developed for RC beams under drop weight impact by using fiber beam section analysis method to predict the impact force. The developed 2DOF analytical model is validated by drop weight impact test results. With the validated analytical model, a simplified model of impact force profile is then proposed by determining six characteristic points, which are expressed by empirical equations fitted by the analytical parametric study

results. The simplified impact force profile predicted by the empirical equations shows a good agreement with the test data.

Keywords: Analytical study; Numerical study; Impact force profile; Drop weight; Reinforced concrete beams

Nomenclature

A	Contact area
$A_{c,i}$	Area of concrete fiber
$A_{s,i}$	Area of steel fiber
b	Width of beam section
c_b	Beam damping
c_c	Contact damping
d	Depth of beam section
F_a	Impact peak force
F_b	Resistance of RC beam under concentrated load
F_p	Impact plateau force
k_b	Global stiffness of beam
k_c	Contact stiffness
l	Beam span
l_{eff}	Effective beam span
l_p	Length of plastic hinge
m_b	Mass of RC beam
m_d	Mass of drop weight
M	Bending moment of beam section
N	Axial force of beam section
P_{dyn}^{max}	Dynamic shear capacity of beam section
t_0	Duration of local response
t_a	Time at peak force
t_b	Duration of primary impact
t_{cd}	Duration of force plateau
t_e	Total impact duration
u_i	Displacement in governing equations
$\dot{u}_i$	Velocity in governing equations
$\ddot{u}_i$	Acceleration in governing equations
v_0	Initial velocity of drop weight
v_b	Velocity of beam at midspan
v_d	Velocity of drop weight
$Z_{c,i}$	Coordinate of concrete fiber along z-axis
$Z_{s,i}$	Coordinate of steel fiber along z-axis
β	Scale factor for contact stiffness
δ	Deflection of beam section
$\dot{\delta}$	Deflection rate of beam section
δ_b	Deflection of RC beam at midspan
$\varepsilon_{c,i}$	Strain of concrete fiber
$\dot{\varepsilon}_{c,i}$	Strain rate of concrete fiber
ε_N	Section strain at the centroidal y-axis
$\varepsilon_{s,j}$	Strain of steel fiber
$\dot{\varepsilon}_{s,j}$	Strain rate of steel fiber
$\sigma_{c,i}$	Stress of concrete fiber
$\sigma_{s,j}$	Stress of steel fiber
ϕ	Curvature of beam section

$\dot{\phi}$ Curvature rate of beam section

1. Introduction

The study on reinforcement concrete (RC) beam under impact has drawn interests of many researchers due to the increasing numbers of natural or man-induced extreme events [1-3]. Drop weight impact test is a widely used approach to examine the impact behaviour of RC beams. Upon drop weight impact, the impact force between a drop weight and an impacted beam is measured by a load cell and the displacement at midspan is recorded to examine the dynamic response of beams. RC beams under impact load may experience flexure failure, flexure-shear failure, or local punching shear failure, depending on the impact loading rates, impact load-carrying capacities of beam section and peak impact force [4-6]. The peak impact force is primarily governed by the local contact stiffness of impact zone and impact energy [7]. Moreover, the drop weight impact results in stress waves propagating from the impact point to the beam ends during the local response phase, leading to a change of the effective beam span [8, 9]. Once the whole beam span is mobilized, the beam enters the global response phase and the global stiffness would affect the impact force [10]. Therefore, the impact force influenced by different factors determines the dynamic response and failure of RC beams subjected to drop weight impact.

Impact force profiles of RC beams subjected to drop weight impacts can be categorized into three types [10]. It is found that the classification of the impact force profile type depends on the ratio of drop weight mass to beam mass. Various mass ratios result in different relative velocities between a drop weight and an impacted beam, causing different interactions at the impact zone. To damage RC beams, heavy impact mass is used in the drop weight test and thus the impact force profiles with force plateau (i.e., Type III impact force profile) are often observed in impact test results. As summarized in Fig. 1, the impact force values measured in the drop weight impact test are affected by different factors. Increasing impact energy causes a higher primary peak force [11, 12]. It is worth noting that impact velocity has a more significant effect on the primary peak force than impact mass [7]. Moreover, the contact stiffness, relating to the drop weight test setup (e.g. impact interlayer and drop weight geometry) and contact material property, also affects the peak impact force [13]. The existence of an initial inclination of drop weight and the drop weight head with a smaller radius decrease the contact areas and thus reduce the peak impact force. The stiffer interlayer such as steel plate or load cell placed between a drop weight and a beam increases the contact stiffness, which causes a higher impact force. Although there are many studies on the peak impact force through experiments and numerical simulations [12, 14-16], very limited systematic studies investigating the influencing factors on the impact force plateau have been conducted. A previous study [10] found that the force plateau is related to the global stiffness of beam after the primary impact pulse. Therefore, the factors influencing the global stiffness such as the beam section, beam span, rebar ratio, and boundary condition should be investigated to examine their effects on the impact force plateau. It should be noted that the structural response such as the maximum displacement usually appears at the end of impact force plateau. Therefore, an accurate prediction of impact force profile is essential for structural response analysis.

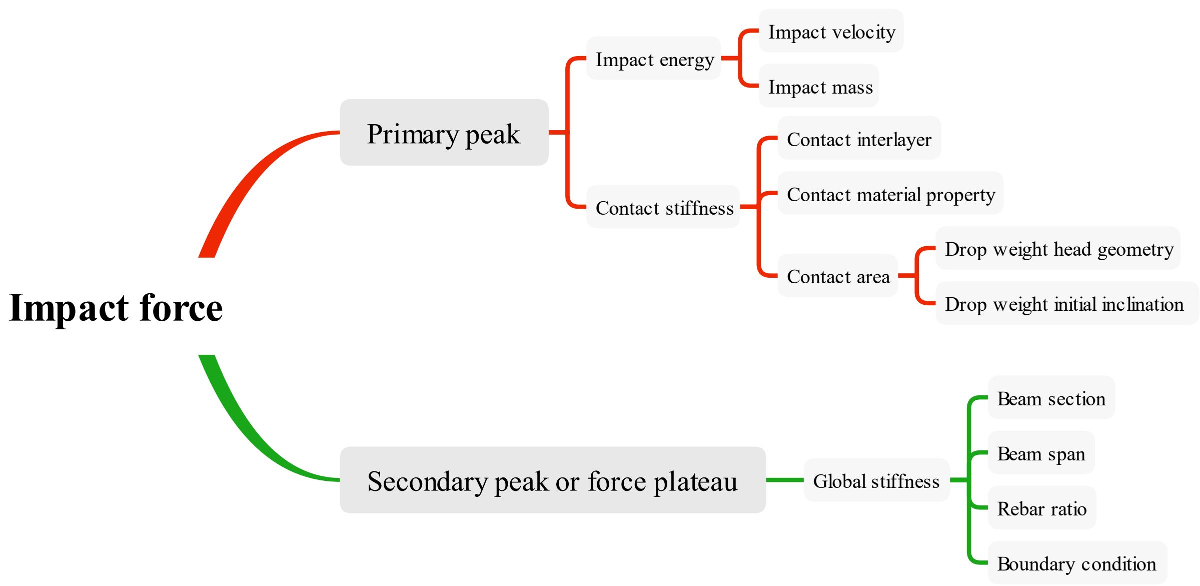

Fig. 1. Factors affecting the impact force profile

Different methods have been employed to study the impact behaviour of RC beam under drop weight impact, i.e., experimental, numerical, and analytical methods [17-22]. The experimental tests allow direct measurement and observation of the impact behaviour of beams. However, it is hard to compare the results from different studies due to different test setups and due to the highly nonlinear nature of results, which causes the results may not be extrapolated [4, 8, 13]. The numerical method provides a technique to predict the impact behaviours of various beams with different test setups. Stress wave propagation along the beam and more results such as stress, strain, and acceleration can be easily retrieved and compared from numerical results [7, 23, 24]. However, it is time-consuming to develop and run high-fidelity numerical models. The analytical methods based on the mass-spring system (SDOF and 2DOF) have been used for the predictions of dynamic responses of beams under impact loads [18, 21, 25]. The impact force and the global response can be obtained by theoretical derivations with some idealizations and assumptions. It should be noted that reasonable assumptions about the characteristics of impact behaviour are very important for the accuracy of the analytical predictions. However, the stress wave propagation along beam, effective beam span, and detailed calculation of global stiffness are not straightforward, hence were not well considered in previous analytical studies.

To date, impact force profile of RC beams under impact loads has not been well studied while the analytical method for fast and accurate prediction on the impact force profile of RC beam is not yet available. In this study, the numerical model is developed in LS-DYNA and calibrated with the testing data of RC beams under drop weight impact. The verified numerical models are employed to study and to quantify the effect of the global stiffness of RC beams, i.e., beam span and boundary condition, on the impact force plateau. Moreover, a 2DOF analytical model is developed for RC beams under drop weight impact by considering stress wave propagation. The developed 2DOF analytical model is validated by the drop weight impact test results. With the validated analytical model, large amounts of impact force data are generated for the development of a simplified impact force profile model. Empirical equations for the simplified impact force profile model are proposed by considering the key factors affecting the impact force. The impact force profiles predicted by the proposed equations are also compared with the test results from other studies to further verify its accuracy.

2. Previous drop weight impact tests

To calibrate the numerical model of RC beam under impact loads, three specimens as listed in Table. 1 were selected from the drop weight impact tests conducted by Fujikake et al. [26].

The drop weight impact setup and the dimension of the RC beam are shown in Fig. 2. The pin-supported RC beam was impacted by a steel drop weight with a mass of 400 kg falling from a height of 1.2 m. A total of four longitudinal rebars are placed in the beam section and the arrangement of longitudinal rebar for three beams is present in Table. 1. The 10 mm-diameter stirrups were placed along the beam at a space of 75 mm. The detailed material strength of concrete and steel rebar can be found in Ref. [26] for each specimen.

Table 1. Arrangement of longitudinal rebar [26].

Specimen	Compression side		Tension side	
	Number and diameter (mm)	Area A_s' (mm^2)	Number and diameter (mm)	Area A_s (mm^2)
S1616-1.2	2*D16	397	2*D16	397
S2222-1.2	2*D22	774	2*D22	774
S1322-1.2	2*D13	126.7	2*D22	774

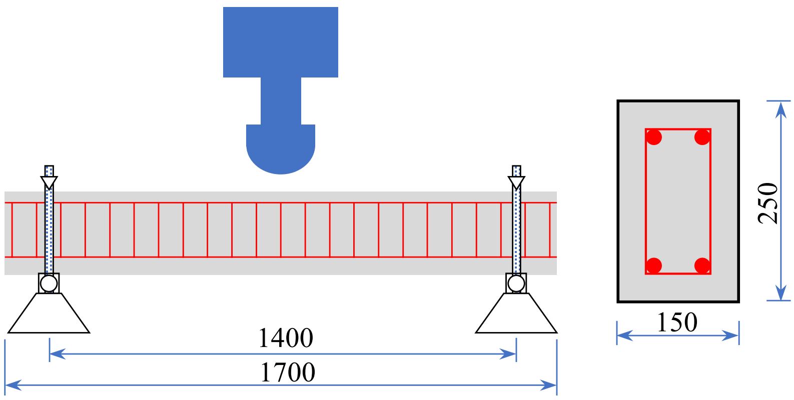

Fig. 2. Test setup and dimension of RC beam (unit: mm) [26].

3. Numerical study of the impact force profile

3.1. Numerical model and calibration

3.1.1. Numerical model

The numerical model is developed in LS-DYNA. The concrete beam and drop weight are simulated by 8-node solid elements. The non-linear beam elements are used to simulate the longitudinal rebars and stirrups. Penalty-based surface-to-surface contact is assigned between the concrete beam and drop weight. The interaction between concrete and reinforcements is defined by the constraint-based coupling method. The mesh size of 10 mm for the numerical model is adopted by conducting a mesh convergence study to obtain reliable results with reasonable computational time.

The concrete material is modelled by the concrete damage model (Mat_72R3) and the piecewise linear plasticity steel model (MAT_24) is employed to simulate the steel longitudinal rebars and stirrups, as commonly used in the numerical simulations [27, 28]. To consider the strain rate effect of concrete and steel under impact loading, the dynamic increase factors (DIFs) are defined for concrete material and steel material, respectively [29, 30]. In addition, the steel drop weight is modelled by the elastic material model (MAT_1).

3.1.2. Comparisons between numerical and test results

Three specimens S1616-1.2, S2222-1.2, S1322-1.2 with different longitudinal rebar ratios in Ref. [26] are employed to calibrate the numerical model. The drop weight falls from a height of 1.2 m, generating a velocity of 4.85 m/s. The numerical result is compared with the test results to validate the numerical models in terms of the impact force and displacement at midspan as shown in Fig. 3. It is found the predicted impact force profiles and displacements at midspan agree well with the test results. Therefore, the developed numerical model is proven yielding reliable predictions of the responses of RC beams subjected to drop weight impact.

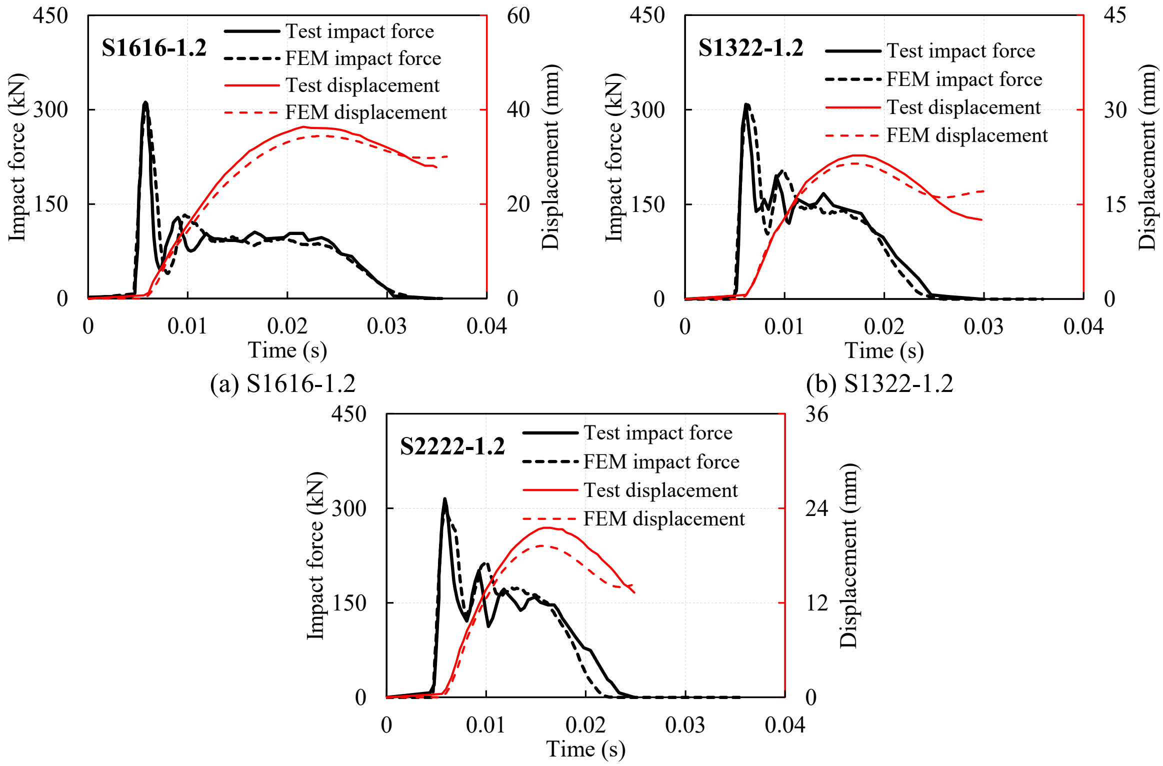

(a) S1616-1.2 (b) S1322-1.2 (c) S2222-1.2

Fig. 3. Comparisons of test [26] and FEM results.

3.2. Numerical study of the global stiffness effect on the impact force profile

It has been demonstrated in a previous study that global stiffness affects the force plateau of the impact force profile [10]. By assuming the global stiffness of a beam as a spring element k_b, the beam under drop weight impact can be simplified as a mass-spring system as shown in Fig. 4. At the end of the primary impulse, the velocity of beam reaches its maximum and begins to decrease due to the resistance provided by the global stiffness of the beam. The relative velocity between drop weight and beam becomes smaller and the velocity and displacement of beam at midspan and drop weight are comparable during the stage of impact force plateau, which causes the midspan part of the beam and drop weight moving together [10]. When the global stiffness k_b in Fig. 4 is greater, the interaction between the drop weight and the beam would be more intensive, which results in a higher impact force plateau. The global flexural stiffness of beam is governed by the flexural stiffness *EI*, beam span *l,* and boundary condition, which can be expressed in Eq. (1) and Eq. (2) for pinned and fixed end, respectively. The effects of beam span and boundary condition on the impact force plateau are analyzed in the subsequent sections.

For pinned end $$k_b = \frac{48EI}{l^3} \tag{1}$$

For fixed end $$k_b = \frac{192EI}{l^3} \tag{2}$$

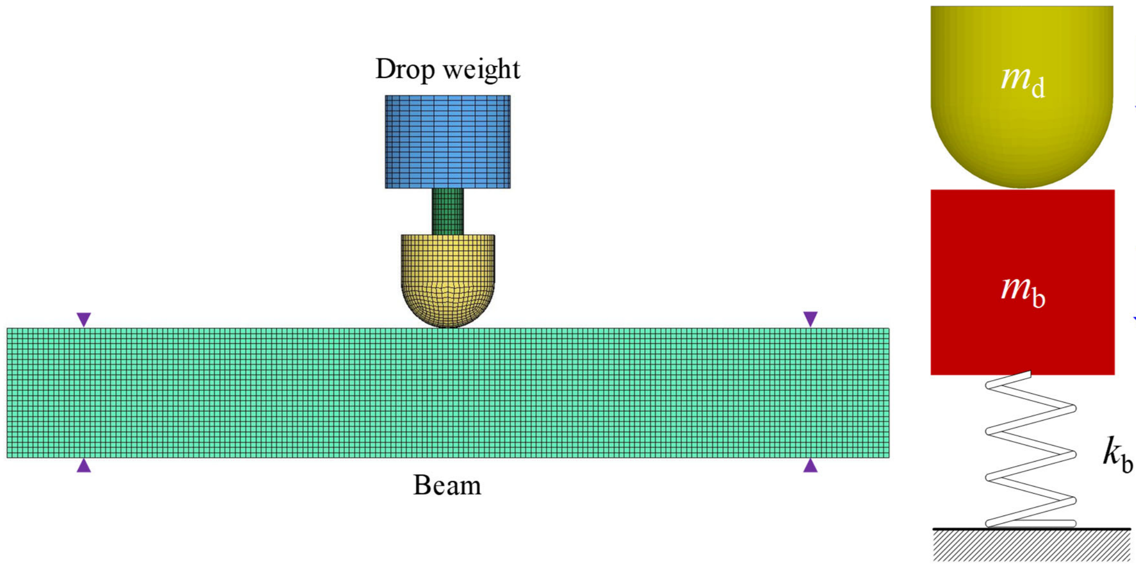

Fig. 4. Illustration of beam under drop weight impact.

3.2.1. Effect of the beam span

The effect of the beam span on the impact force profile is studied in this section. Five beams with the beam span of 1.4 m, 2.1 m, 2.8 m, 3.5 m, and 4.2 m are considered. The beams have the same section dimension and rebar layout as specimen S1616-1.2 as shown in Fig. 2. Two sets of impact scenarios are considered as given in Table 2, which includes the beams subjected to impact with a constant impact mass ratio of 3.0 (the beam mass increases with the beam span) and the beams impacted by a constant impact mass of 400 kg.

Table 2. Impact mass and mass ratio.

Impact scenario	Beam span / m	Impact mass / kg	Beam mass / kg	Mass ratio
Impact with constant mass ratio	1.4	400.0	131.3	3.0
	2.1	590.6	196.9	
	2.8	787.5	262.5	
	3.5	984.4	328.1	
	4.2	1181.3	393.8	
Impact with constant mass	1.4	400	131.3	3.0
	2.1		196.9	2.0
	2.8		262.5	1.5
	3.5		328.1	1.2
	4.2		393.8	1.0

3.2.1.1. Impacted by a constant mass ratio

Increasing the beam span inevitably causes the increase of beam mass, which results in a decrease of mass ratio of drop weight to beam given the same impact mass. Since the mass ratio affects the impact force profile, a constant mass ratio of 3.0 is adopted first in this study to investigate the effect of span on impact force plateau. The impact mass and mass ratio for the specimens with different clear spans are listed in Table 2.

The impact force of the beams under a constant impact mass ratio of 3.0 is illustrated in Fig. 5. As shown, in the primary force stage, the peak impact force F_a increases from 302.06 kN to 405.22 kN due to the increase of impact mass (i.e. impact energy). After the primary pulse, there are force fluctuations due to the interaction between the drop weight and the beam. After the transitional stage, the drop weight and beam move together and the relative velocity between them is almost zero. The impact force keeps an almost constant value F_p that can be defined as the average impact force during the plateau stage. The plateau force F_p drops from

93.17 kN to 31.90 kN, with a decrease of 65.76%, as the beam span increases from 1.4 m to 4.2 m, but the corresponding duration of the plateau stage becomes longer with the increased beam span.

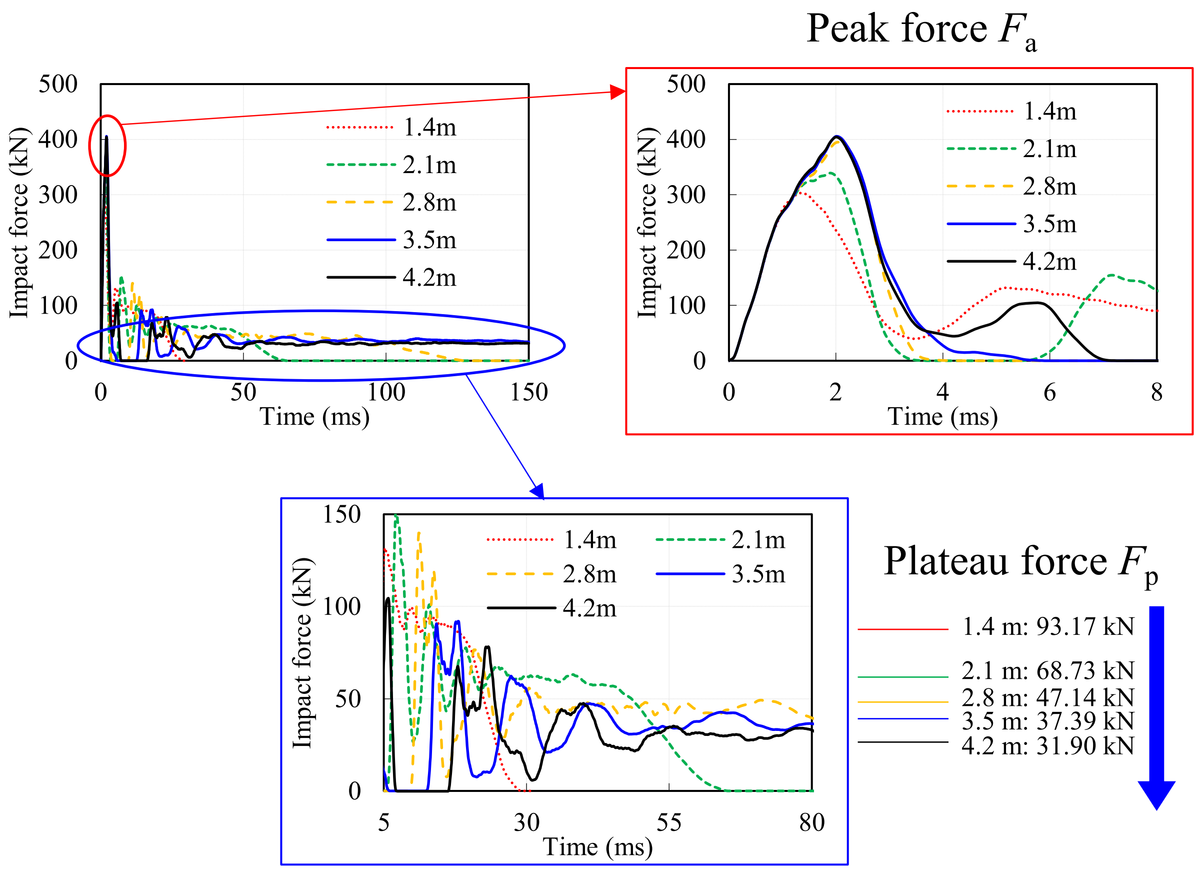

Fig. 5. Impact force acting on the beams with different spans under constant impact mass ratio of 3.0.

3.2.1.2. Impacted by a constant mass

To further investigate the effect of the beam span on the impact force profile, five beams are impacted by the drop weight with a constant mass of 400 kg (i.e. the mass ratio varied from 3.0 to 1.0 as listed in Table 2). The impact force time history is presented in Fig. 6. The primary force peaks of the specimens are similar, indicating that the span has negligible effect on the primary force peak, which has been also verified by Pham and Hao [31]. In the plateau stage, however, the plateau force decreases by 72.07%, from 93.17 kN to 26.02 kN. With the increase of beam span, the duration of the plateau stage becomes longer. Therefore, increasing the beam span causes decrease of plateau force and increase of plateau stage duration due to the decrease of the global stiffness.

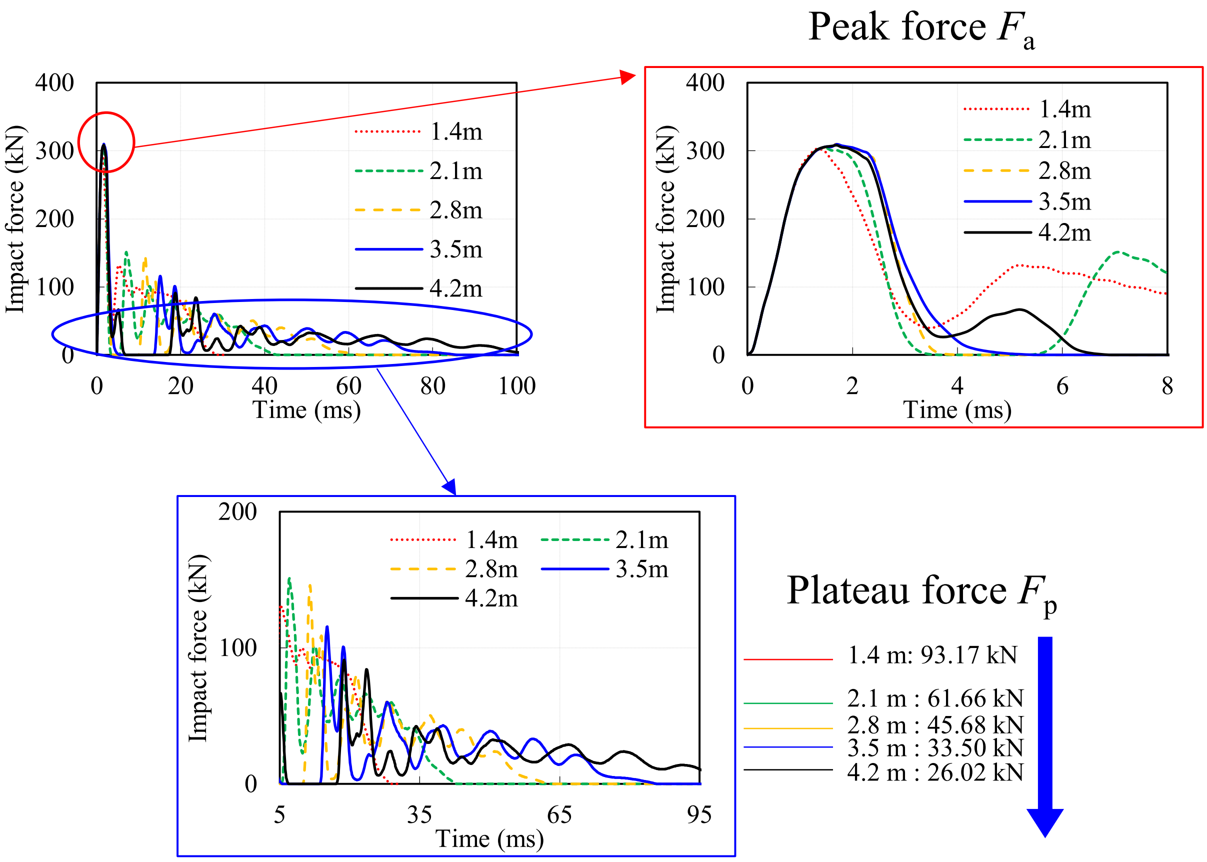

Fig. 6. Impact force acting on the beams with different spans under constant impact mass of 400 kg.

3.2.2. Effect of the boundary condition

The responses of RC beams with pinned and fixed boundary conditions are compared as shown in Fig. 7. The effective span of 2.8 m, 3.5 m, and 4.2 m are considered. The impact velocity of the drop weight is 4.85 m/s. The mass ratio of drop weight to beam remains 3.0 and the impact mass is listed in Table 2 for the beams with different spans. The time histories of impact force are shown in Fig. 8. Even though the beams with the same span have different boundary conditions in each group, the primary force peaks are similar as shown in Fig. 8(a)~(c).

It indicates that the primary force peaks are independent of the boundary conditions. This result is supported by the previous study [31] which showed the boundary condition does not affect the peak impact force. The peak impact force depends on the impact mass, impact velocity, and contact stiffness [13]. A higher plateau force appears in the fixed end beam than the pin-supported beam. For example, for the beams with a span of 2.8 m as shown in Fig 8(a), the plateau force of the fixed beam (141.02 kN) is larger than that of the pin-supported beam (47.14 kN).

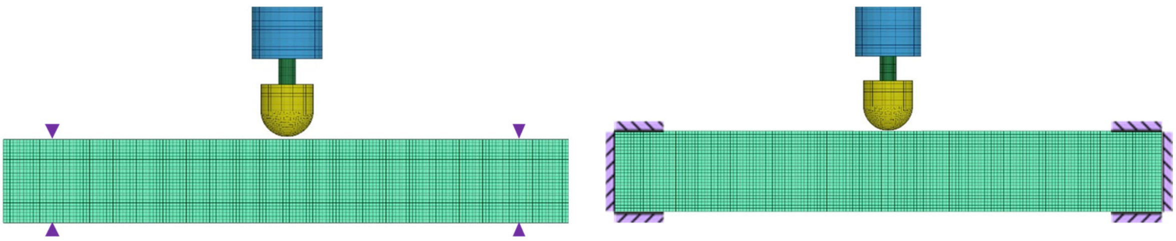

(a) Pinned end (b) Fixed end

Fig. 7. Numerical models of the beams with different boundary conditions.

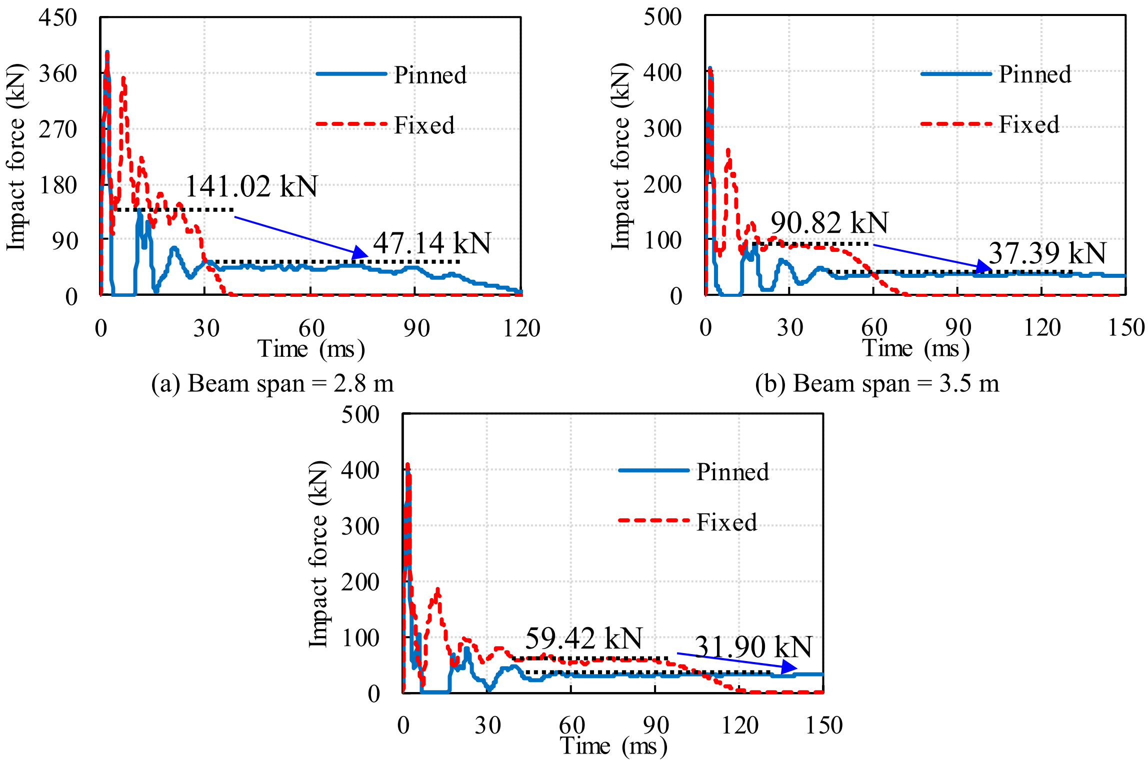

(a) Beam span = 2.8 m (b) Beam span = 3.5 m

(c) Beam span = 4.2 m

Fig. 8. Impact force acting on the beams with different boundary conditions.

3.2.3. Discussion of the global stiffness effect on the impact force profile

Given the same input impact energy, the primary force peaks are similar for the specimens regardless of the beam clear span and boundary condition, which agree with the results in Refs. [4, 31]. However, the plateau force decreases with the reduction of beam global stiffness (i.e. increasing the beam span or using the less-constrained boundary condition), but duration increases. Moreover, by analyzing the test results presented in Fig. 3, the specimen S2222-1.2 with a higher tensile reinforcement ratio of 2.02% experiences a larger plateau impact force of 156.18 kN because of its larger global stiffness, compared to that of 95.66 kN in the specimens S1616-1.2 with a tensile reinforcement ratio of 1.07%. Therefore, it is evident that the beam with lower global stiffness provides lower resistance which weakens the interaction between the drop weight and beam and thus causes a lower plateau force. The duration of the force plateau becomes longer for the specimen with lower global stiffness as shown in Fig. 3, Fig. 5, Fig. 6, and Fig. 8. This is because the lower global stiffness leads to a less beam resistance to stop the downward movement of the beam and the drop weight. A longer time is needed to reduce the velocity of the beam to zero and to reach its maximum midspan displacement. It is concluded that the global stiffness has negligible effect on the primary force peak but has significant influence on the plateau force. Based on this conclusion and other studies on the factors affecting the impact force [10, 13], a simplified impact force profile model is proposed by considering these influencing factors in the subsequent analytical study.

4. Analytical study of the impact force profile

4.1. Analytical model

4.1.1. 2DOF model

To develop a proper simplified impact force profile model, various factors affecting impact force as listed in Fig. 1 are considered in the analytical model based on a 2DOF mass-spring-damping system. Since the impact response consists of the local response at the impact zone and the global response of a beam [12, 18, 31], the pin-supported beam under drop weight impact can be simplified as the 2DOF mass-spring-damping system as shown in Fig.9. The drop weight and beam are assumed as two lumped masses, and the local contact stiffness and the global stiffness of beam are assumed as two springs. The analytical model is explained in detail in the following section and the applicability of the model is discussed in section 4.4.

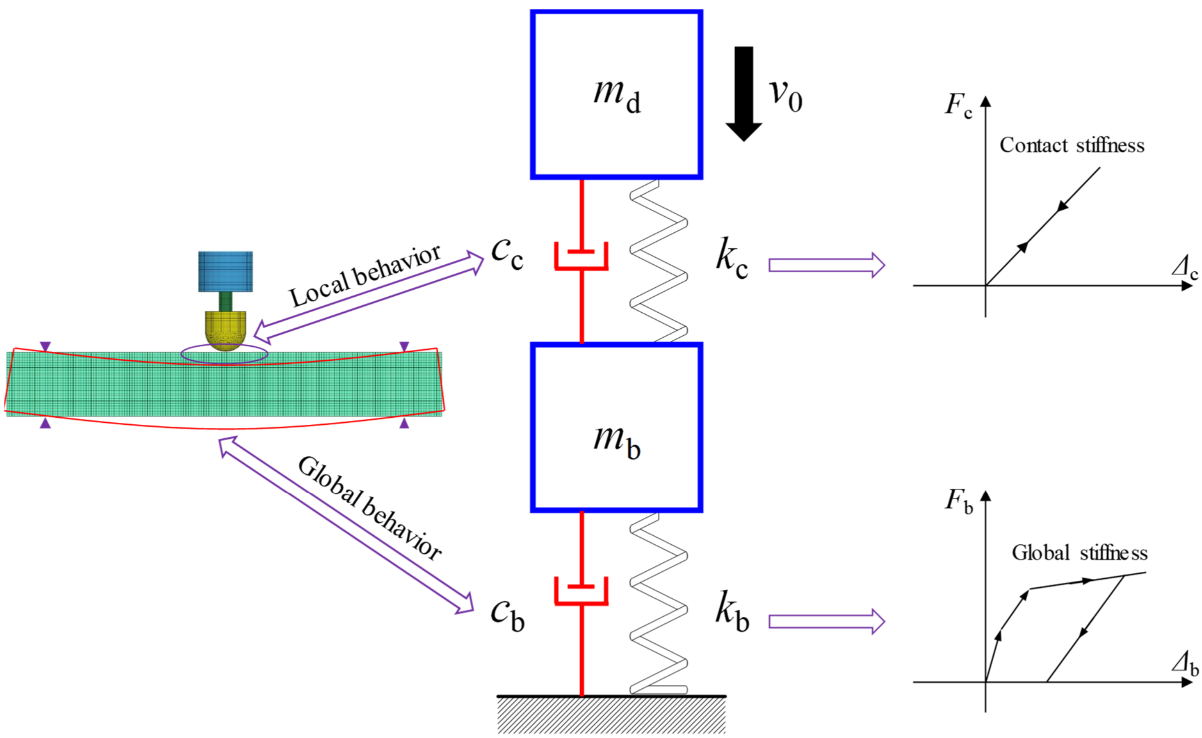

Fig. 9. 2DOF model of an RC beam under drop weight impact.

The governing equations of the 2DOF mass-spring-damping system are expressed as follows:

$$m_d\ddot{u}_d + c_c(\dot{u}_d - \dot{u}_b) + k_c(u_d - u_b) = 0 \quad (3)$$

$$m_b\ddot{u}_b + c_b\dot{u}_b + c_c(\dot{u}_b - \dot{u}_d) + k_b u_b + k_c(u_b - u_d) = 0 \quad (4)$$

where u_i, $\dot{u}_i$, and $\ddot{u}_i$ ($i = d$ or b) are the displacement, velocity, and acceleration of the drop weight or beam mass, respectively. The parameters include the initial impact velocity of the drop weight v_0, drop weight mass m_d, contact stiffness k_c, contact damping c_c, effective mass of the beam m_b, global stiffness of the beam k_b, and beam damping c_b. Herein, the initial impact velocity v_0 and drop weight mass m_d can be determined by the designed impact energy. Moreover, selecting an appropriate contact law is important to predict impact force for the local contact of impact. Based on the Hertzian contact theory, pure elastic contact model and dissipative visco-elastic contact model were developed [32-34]. The dissipative visco-elastic contact model considers the energy loss during the impact by using the contact damping and it is used to predict contact force for impact actions [35, 36]. In this study, the contact stiffness and contact damping are incorporated into the analytical 2DOF model as shown in Fig. 9. The contact stiffness (k_c) is related to the contact area, drop weight head geometry, and contact material properties [13, 37, 38]. In regard to a flat head, the contact stiffness is calculated by using an equation similar to the penalty contact algorithm in LS-DYNA [39] as follows:

$$k_c = \beta\frac{EA}{h} \quad (5)$$

where E and A are Young's modulus of concrete and contact area, respectively, h is the thickness of the contact area, β is a scale factor to adjust the contact stiffness by calibrating the impact force. If the drop weight head has a curved shape, the contact stiffness is defined by using the Hertz contact model [32, 40]. The contact stiffness is expressed as follows:

$$k_c = \beta \frac{4\sqrt{R_{\mathrm{h}}}}{3}\left(\frac{1-\nu_d^2}{E_d}+\frac{1-\nu_b^2}{E_b}\right)^{-1} \tag{6}$$

where R_{h} is the radius of the curved head, E_{d} and E_{b} are Young's modulus of drop weight and beam, respectively, ν_{d} and ν_{b} are Poisson's ratio of drop weight and beam, respectively. Moreover, the contact damping should be considered to avoid the intensive oscillation of the impact force [20, 41]. The contact damping c_{c} proposed by Anagnostopoulos [42] is adopted and expressed as follows:

$$c_c = 2\xi_{\mathrm{c}}\sqrt{\frac{m_d m_b k_c}{(m_d + m_b)}} \tag{7}$$

where ξ_{c} is the contact damping ratio and is determined as 0.2 by calibrating the test results, c_{b} is the damping of RC beam for the global response stage and the damping ratio is assumed to be 5%.

During an impact event, the beam is mobilized with the increased effective beam span l_{eff} as stress waves propagate from the impact location to the boundaries as shown in Fig. 10. P-wave, shear wave and Rayleigh surface wave are generated in the beam. P-wave arrives the supports first and then shear wave and Rayleigh wave comes last. P-wave causes the longitudinal vibration while shear wave propagates transversely and causes the vertical vibration of beam, which induces vertical reaction force and response. After reaching the boundary, shear stress wave reflects and travels back to the impact location, then it is assumed that the whole beam span is mobilized and the global response is activated in this study.

Therefore, the duration of local response stage t_0 can be determined by using the beam span l and the velocity of shear stress wave v_s [7, 43] as follows:

$$t_0 = \frac{l}{v_s} \tag{8}$$

The shear stress wave velocity v_s can be calculated by:

$$v_s = \sqrt{\frac{E}{2\rho(1+\mu)}} \tag{9}$$

where E, ρ, and μ are Young's modulus, density, and Poisson's ratio of concrete. During the local response stage, it is assumed that the effective beam mass increases linearly as the increase of the effective beam span l_{eff} by considering the stress wave propagation. When the whole beam is mobilized in the global response stage after the duration of t_0, the effective beam mass keeps constant [44] as follows,

$$m_b = 0.493\rho bdl \tag{10}$$

where ρ is the density of an RC beam, b and d are the width and depth of beam section, respectively. In addition, the global stiffness of a beam k_b describing the relationship of resistance (F_b) and deflection (δ_b) is determined by beam section analysis as illustrated in section 4.1.2.

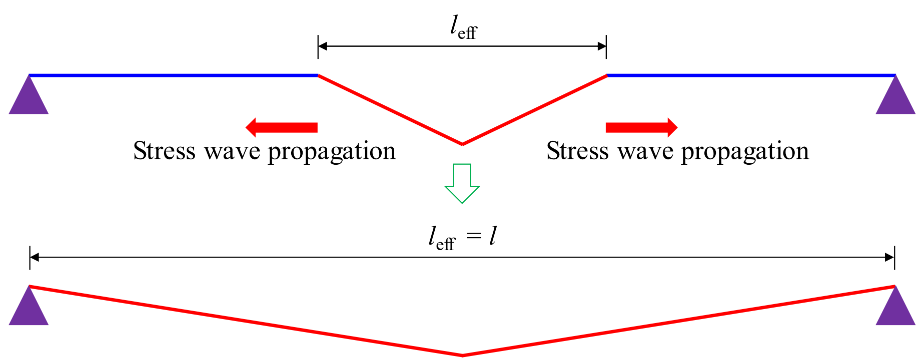

Fig. 10. Stress wave propagation and effective span of RC beam.

4.1.2. Beam section analysis

A nonlinear fiber beam section analysis of a pin-supported RC beam is conducted to determine the global stiffness of beam subjected to a concentrated load in this section. The relationship of moment (M) and curvature (ϕ) of beam section is calculated firstly by the nonlinear analysis. Then the relationship of resistance (F_b) and deflection (δ_b) is obtained by using the moment-curvature relationship (M-ϕ) and the resistance-deflection relationship (F_b-δ_b) is used to give the global behaviour of an RC beam under impact loads.

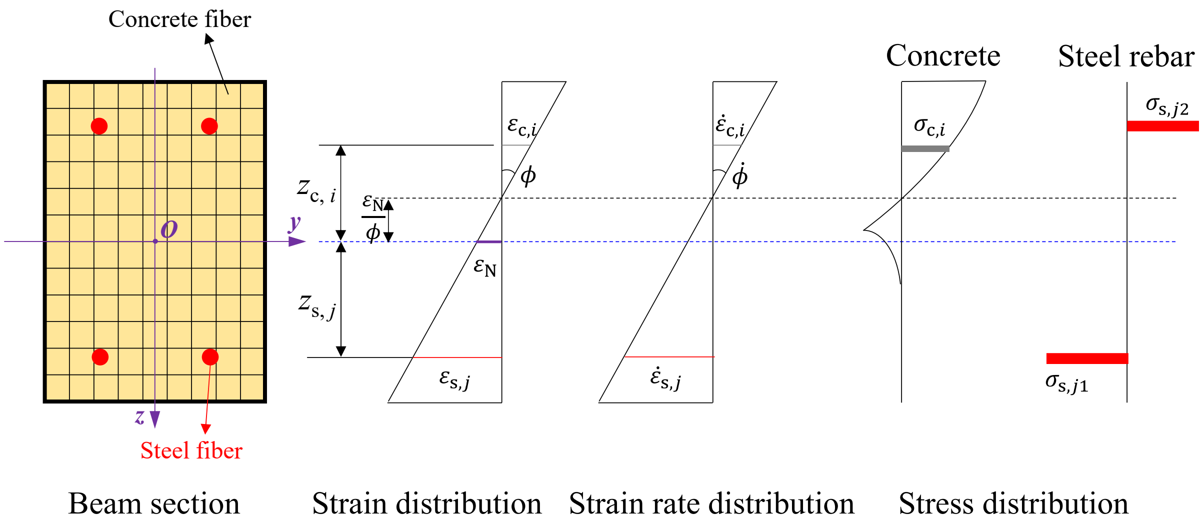

Fig. 11. Schematic diagram of fiber beam section and distribution of strain, strain rate, and stress.

The fiber beam section analysis method is employed as shown in Fig. 11. The section of an RC beam is divided into concrete fibers and steel rebar fibers and a perfect bonding between concrete fiber and steel rebar fiber is assumed. As shown in Fig. 12(a), the modified Kent-Park concrete model is adopted for concrete fibers [45, 46]. This concrete model is widely used for the fiber beam section analysis in OpenSees and ABAQUS [47, 48]. The concrete compressive stress is expressed as a function of concrete strain as follows:

$$\sigma = \begin{cases} Kf_c'\left[2\left(\frac{\varepsilon}{\varepsilon_0}\right) - \left(\frac{\varepsilon}{\varepsilon_0}\right)^2\right] & (\varepsilon \le \varepsilon_0) \\ Kf_c'[1 - Z(\varepsilon - \varepsilon_0)] & (\varepsilon_0 < \varepsilon \le \varepsilon_u) \\ 0.2Kf_c' & (\varepsilon > \varepsilon_u) \end{cases} \tag{11a}$$

$$\varepsilon_0 = 0.002K \tag{11b}$$

$$K = 1 + \frac{\rho_s f_{yh}}{f_c'} \tag{11c}$$

$$Z = \frac{0.5}{\frac{3 + 0.29f_c'}{145f_c' - 1000} + 0.75\rho_s\sqrt{\frac{h'}{s_h}} - 0.002K} \tag{11d}$$

$$\varepsilon_u = 0.004 + 0.9\rho_s\left(\frac{f_{yh}}{300}\right) \tag{11e}$$

where f_c' is the concrete compressive strength, K is a variable considering the increase of compressive strength by stirrup confinement, ε_0 and ε_u are the concrete strain corresponding to the maximum stress and the ultimate stress, ρ_s is the stirrup ratio and f_{yh} is the yield strength of stirrups, Z is the strain-softening slope, h' is the width of concrete core confined by stirrups, and s_h is the center spacing between stirrups. Moreover, a bilinear model is adopted to illustrate the tension behaviour of concrete as shown in Fig. 12(a). σ_{t0} and ε_{t0} are the tensile strength and strain of concrete, respectively.

The steel material model proposed by Esmaeily and Xiao is employed for steel rebar as shown in Fig. 12(b) [49]. The relationship of stress and strain for steel is given as follows,

$$\sigma = \begin{cases} E_s\varepsilon & (\varepsilon \le \varepsilon_y) \\ f_y & (\varepsilon_y < \varepsilon \le k_1\varepsilon_y) \\ k_4 f_y + \frac{E_s(1 - k_4)}{\varepsilon_y(k_2 - k_1)^2}\left(\varepsilon - k_2\varepsilon_y\right)^2 & (\varepsilon > k_1\varepsilon_y) \end{cases} \tag{12}$$

where E_s, f_y, and ε_y are Young's modulus, yield strength, and yield strain of steel material, respectively, k_1, k_2, k_3, and k_4 are the parameters that control the shape of strain-stress curve as presented in Fig. 12(b).

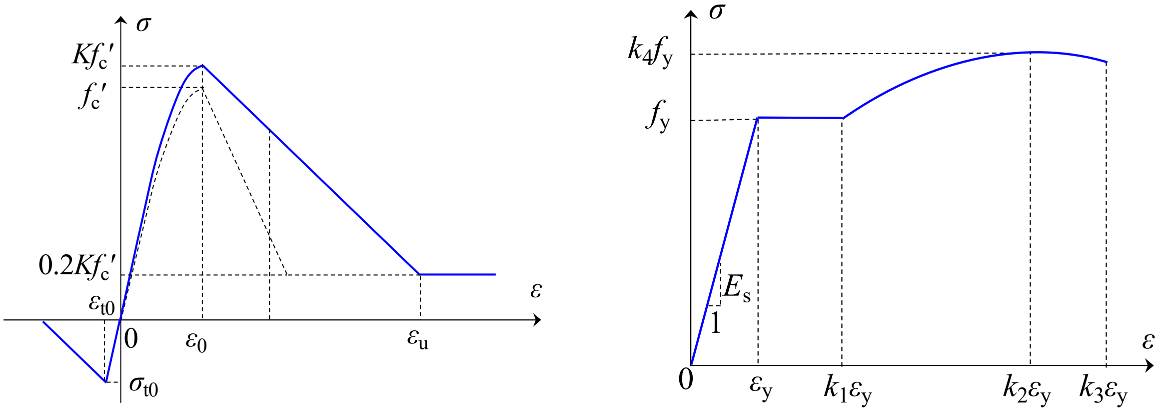

(a) Concrete model (b) Steel material model

Fig. 12. Material models for concrete and steel.

To account for the strain rate effect on the material strengths, the DIFs for concrete and steel are employed [29, 30]. The strain rate of concrete and steel rebar can be calculated by using the curvature rate of beam section $\dot{\phi}$ as presented in Fig. 11.

Since the impact force can be deemed as a concentrated load acting on the RC beam at midspan, the simplified model for calculating the deflection δ of beam under concentrated load at midspan is illustrated in Fig. 13. The relationship between curvature ϕ of the beam section at midspan and deflection δ at midspan in the elastic and plastic stage [20, 21, 50] can be expressed as follows:

Elastic stage $$\phi = \frac{12}{l^2}\delta \quad \text{for } 0 < \delta \le \delta_y \tag{13}$$

Plastic stage $$\phi = \phi_y + \frac{4}{l \cdot l_p}(\delta - \delta_y) \quad \text{for } \delta > \delta_y \tag{14}$$

where δ_y is the yield deflection, l is the beam clear span, and l_p is the length of the plastic hinge at midspan and can be calculated by the following equation proposed by Mattock [51],

$$l_p = d + 0.05l \tag{15}$$

where d is the depth of beam section. Therefore, the relationships of curvature rate $\dot{\phi}$ of beam section and deflection rate $\dot{\delta}$ (i.e., loading rate) are given as follows,

Elastic stage $$\dot{\phi} = \frac{12}{l^2}\dot{\delta} \quad \text{for } 0 < \delta \le \delta_y \tag{16}$$

Plastic stage $$\dot{\phi} = \frac{4}{l \cdot l_p}\dot{\delta} \quad \text{for } \delta > \delta_y \tag{17}$$

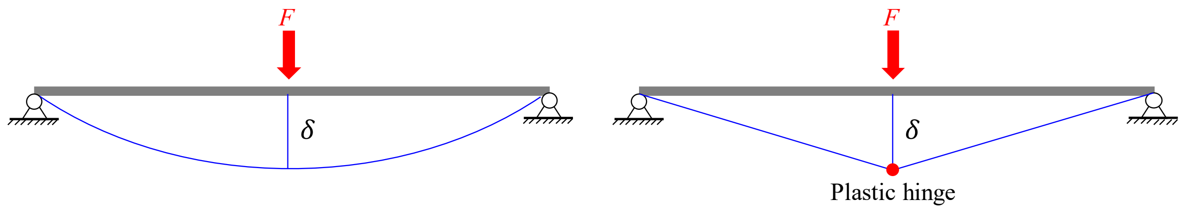

(a) Elastic defection (b) Plastic defection

Fig. 13. Deflection of an RC beam under concentrated load at midspan.

With the plane section assumption, i.e., the beam section remains plane under loading, the strain and strain rate distributes linearly along the beam depth as shown in Fig. 11. According to the curvature ϕ and curvature rate $\dot{\phi}$ of beam section, the strain ε_i and strain rate $\dot{\varepsilon}_i$ of concrete fiber or steel fiber can be derived as follows,

$$\varepsilon_i = \varepsilon_N + \phi Z_i \tag{18}$$

$$\dot{\varepsilon}_i = \left(\frac{\varepsilon_N}{\phi} + Z_i\right)\dot{\phi} \tag{19}$$

where ε_N is the section strain at the centroidal y-axis, Z_i is the coordinate of concrete fiber ($Z_{c,i}$) or steel fiber ($Z_{s,i}$) along z-axis of the beam section. The stress of concrete fiber ($\sigma_{c,i}$) and steel fiber ($\sigma_{s,j}$) can be calculated with the strain and the corresponding strain rate from the material constitutive model and DIF model. Based on the areas of section fiber (concrete fiber ($A_{c,i}$) and steel fiber ($A_{s,i}$)) and stress of section fibers, the axial force (N) and bending moment (M) of the beam section are calculated by the equilibrium equations as follows,

$$N = \int \sigma dA = \sum_{i=1}^{m} \sigma_{\mathrm{c},i} A_{c,i} + \sum_{j=1}^{n} \sigma_{\mathrm{s},j} A_{\mathrm{s},j} = 0 \tag{20}$$

$$M = \int \sigma Z_i dA = \sum_{i=1}^{m} \sigma_{\mathrm{c},i} Z_{\mathrm{c},i} A_{\mathrm{c},i} + \sum_{j=1}^{n} \sigma_{\mathrm{s},j} Z_{\mathrm{s},j} A_{\mathrm{s},j} \tag{21}$$

It should be noted that the axial force acting on the beam section is zero in this study. In order to meet the equilibrium for axial force ($N = 0$) as expressed in Eq. (20), the section strain at the neutral y-axis ε_N is determined by iterations. Once ε_N is obtained, the bending moment M can be derived by Eq. (21) and the resistance F_b is calculated sequentially. To get the full section response, the curvature ϕ increases at a step of 0.0004 1/mm as an iterative process. Fig. 14 illustrates the flowchart of beam section analysis to calculate the moment-curvature relationship (M-ϕ) and resistance-deflection relationship (F_b-δ_b) for RC beam. When the resistance-deflection relationship of RC beam is obtained by conducting the section analysis, the global stiffness k_b of RC beam shown in Fig. 9 can be determined accordingly. After defining all parameters employed in the analytical model, the governing equations of 2DOF model as given in Eq. (3) and Eq. (4) are solved by using the SciPy library in Python.

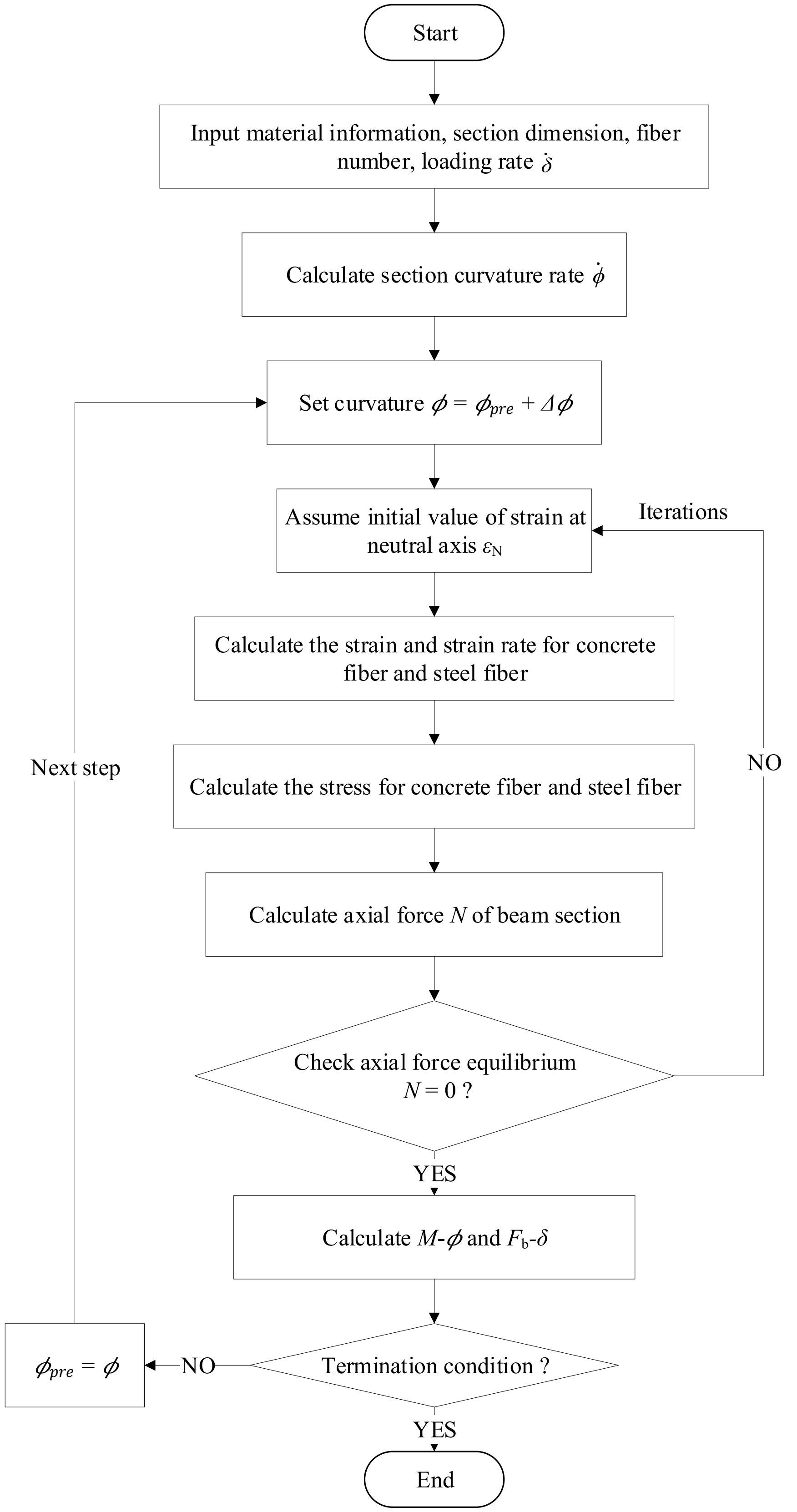

Fig. 14. Flowchart of fiber beam section analysis.

4.1.3. Calibration of the proposed analytical model

Two sets of RC beam tests are employed to calibrate the analytical model, i.e., RC beams subjected to a concentrated load at midspan with various loading rates to calibrate the beam section model, and RC beams under drop weight impact to check the validity of the developed 2DOF model. In terms of the first part of calibration (i.e. beam section analysis model), the RC beams (S1616, S2222, and S1322) tested under different loading rates by Fujikake et al. [26] are used. The dimension, rebar layout, and material strength of the RC beams are presented in Fig. 2 and Table 1. A concentrated load with a loading rate of 0.5 mm/s (static loading) or 2000 mm/s (rapid loading) is applied at midspan of the RC beam and the relationship of the applied load on beam and midspan deflection is captured. By using the beam section analysis as illustrated in Section 4.1.2, the analytical load-deflection relationship is calculated and agrees well with the test result for the specimens under different loading rates as shown in Fig. 15. In addition, it is noted that there are some fluctuations in the test results under a higher loading rate of 2000 mm/s as presented in Fig. 15(b), which is not observed in the analytical results. This is because there are local vibrations between the loading actuator and RC beam at the loading point in the test, while the local interaction is not considered in the beam section analysis. In general, the beam section analysis results are in good agreement with the test results, indicating that the beam section analysis model can be used to calculate the global stiffness of beams in the proposed 2DOF model.

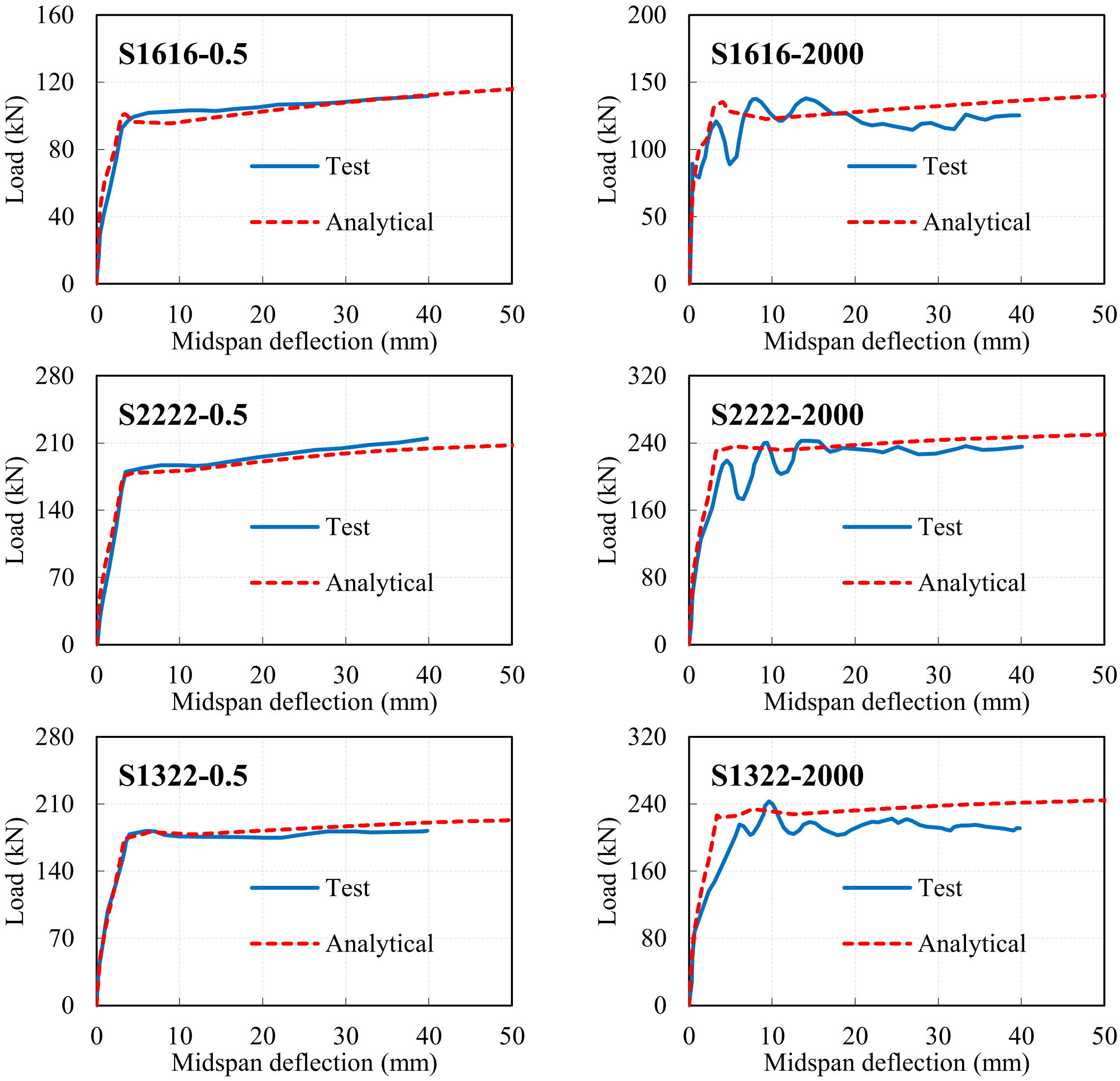

(a) Loading rate of 0.5 mm/s (b) Loading rate of 2000 mm/s

Fig. 15.Comparisons of test [26] and analytical results of RC beams under various loading rates by section analysis.

In addition, the 2DOF analytical model is calibrated by the test data of RC beams under drop weight impact tests [22, 26, 52]. The detailed information of the geometry of beam, rebar layout, and impact energy of the impact tests were reported in the literature. It is worth noting that the contact areas in these tests are different due to different geometries of drop weight head and beam section, causing various contact stiffness k_b. The drop weight head is hemisphere with a radius of 90 mm in Ref. [26] while a flat contact surface with a diameter of 200 mm is employed in the drop weight tests on the beams with width of 150 mm in Ref. [52] and 200 mm in Ref. [22], respectively. Therefore, the smaller contact area in Ref. [26] results in a lower contact stiffness than that in Refs. [22, 52]. The contact stiffness for the tests in the Refs. [22, 26, 52] are determined as 0.8×10^8 N/m, 10×10^8 N/m, and 15×10^8 N/m, respectively, by using Eq. (5) and Eq. (6). The predicted impact force and displacement at midspan are in good agreement with the test results as shown in Fig. 16 (a) and (b). The impact force profile is well predicted as presented in Fig. 16(a) by the analytical method, indicating that the developed 2DOF model can be used to calculate the impact force profile of pin-supported RC beams under drop weight impact.

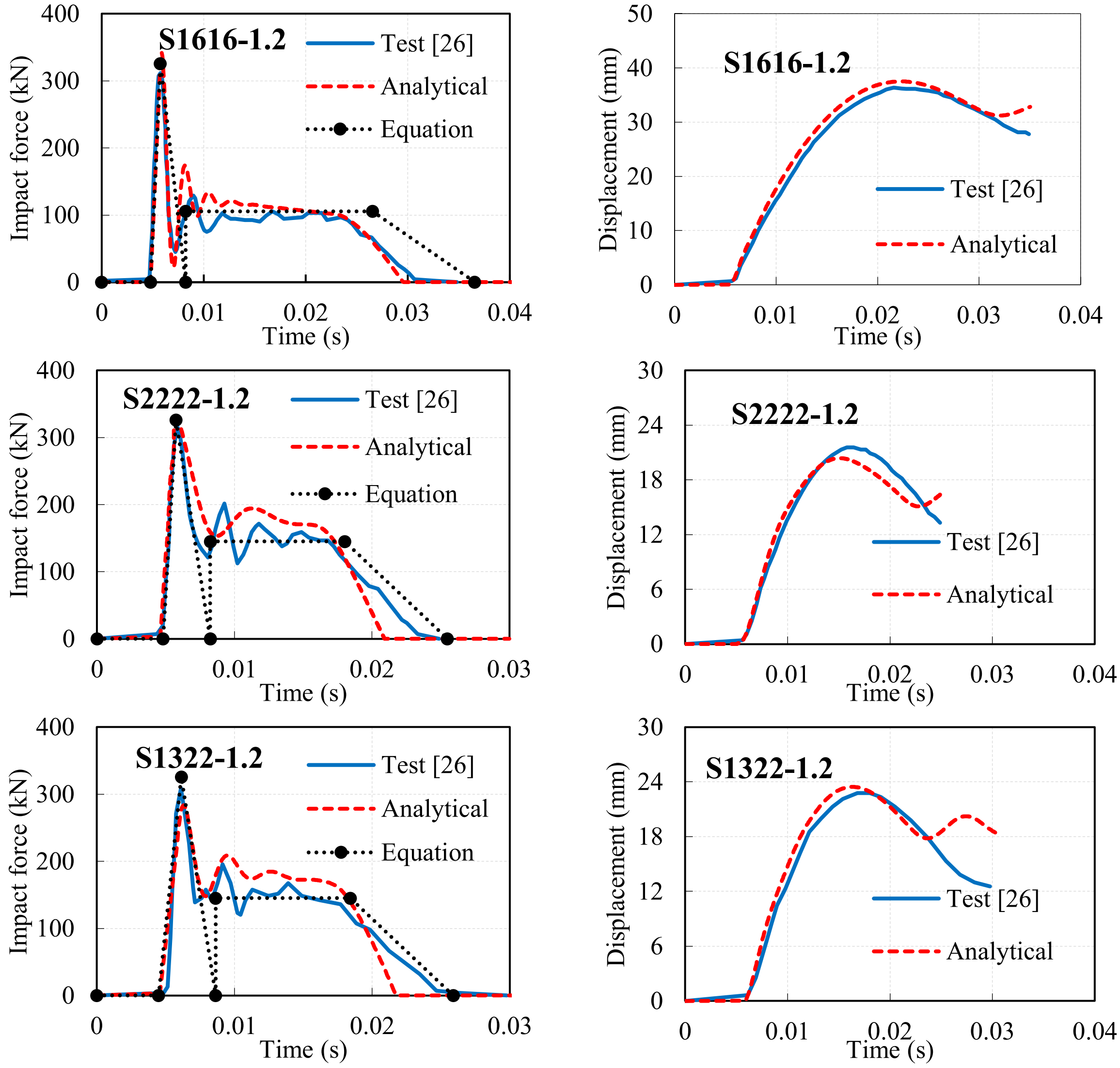

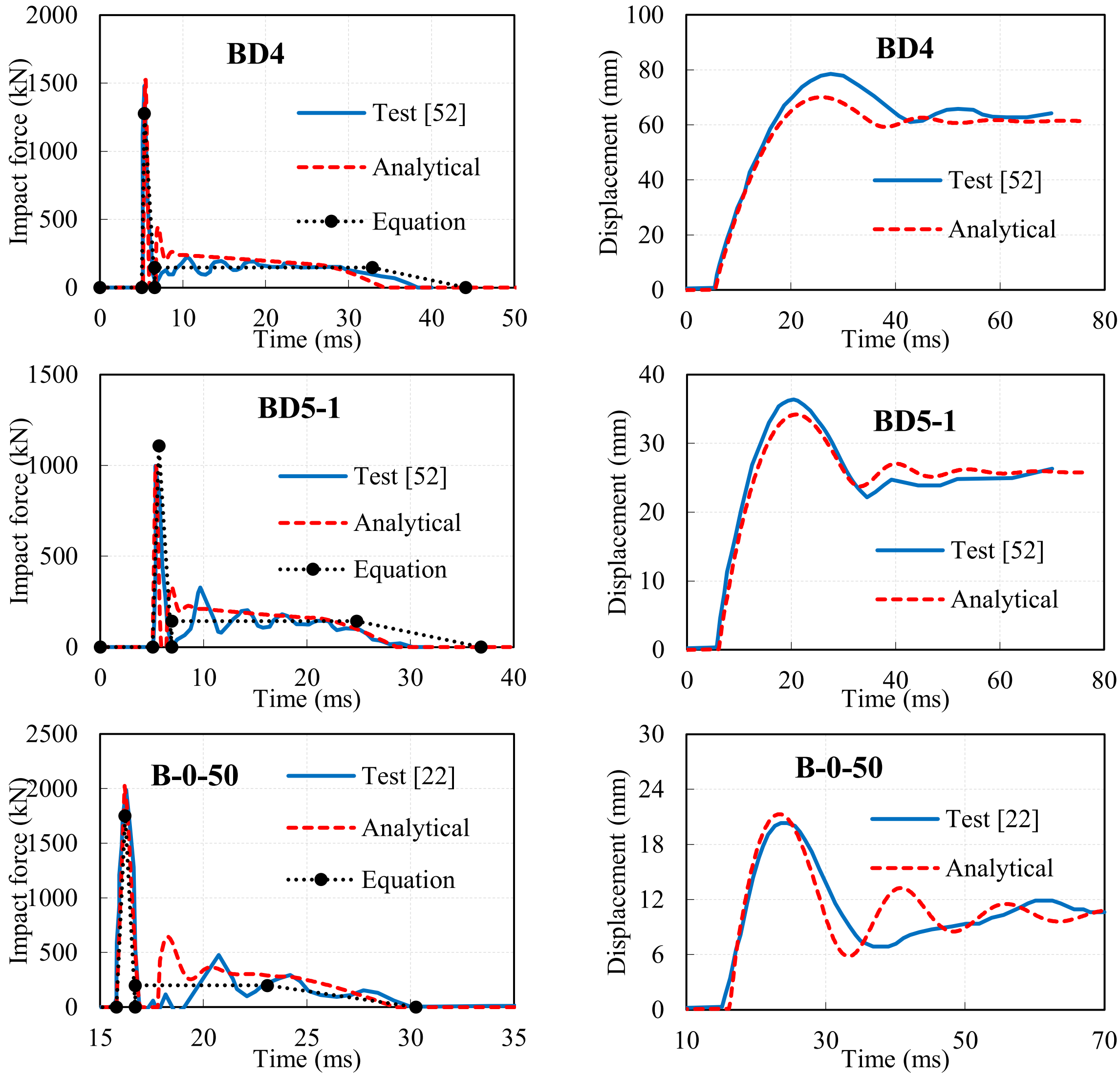

(a) Time history of impact force (b) Time history of displacement

Fig. 16. Comparisons of test results [22, 26, 52], analytical predictions, and results predicted by equations (22)~(27) of RC beams under drop weight impact.

4.2. Development of the simplified impact force profile model

Based on the impact force profiles recorded in test [4, 22, 26, 52, 53], a simplified impact force profile is suggested as shown in Fig 17. It is defined by six characteristic points (*OABCDE*) and composed of a primary triangular area (*OAB*) with the peak impact force F_a and trapezoidal force block (*BCDE*) with a constant plateau force F_p. By considering the key parameters affecting the impact force profile as summarized in Fig. 1, the force (F_a and F_p) and duration (t_a, t_b, t_{cd}, and t_e) of the characteristic points as presented in Fig 17 can be determined by using the fitted equations (22)~(27) derived from the analytical results.

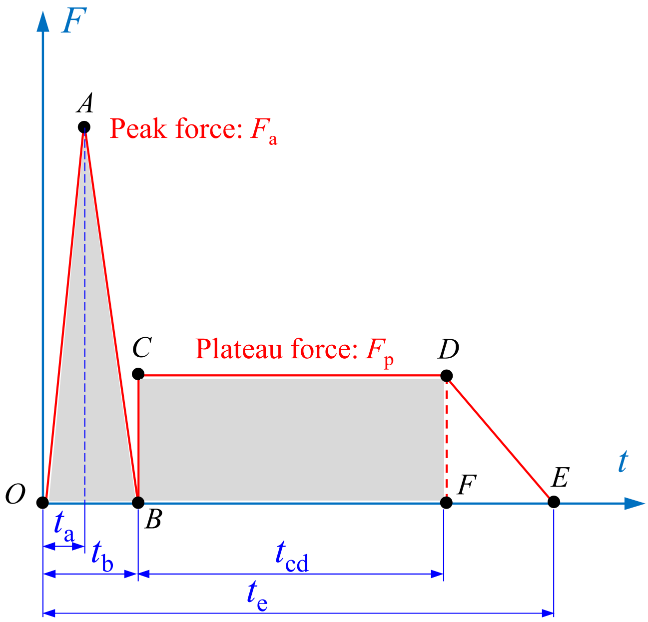

Fig. 17. Simplified impact force profile (unit: t/ms, F/kN).

Table 3. Parameters used for analytical study.

Parameters	Values
Impact mass m_d (kg)	200, 300, **400**, 500,600, 800, 1000, 1200, 1400, 1600, 1800
Impact velocity v_0 (m/s)	1.0, 2.0, 3.0, 4.0, **5.0**, 6.0, 7.0, 8.0, 9.0, 10.0
Contact stiffness k_c (10^8 N/m)	0.05, 0.08, 0.1, 0.2, 0.5, **0.8**, 1.0, 2.0, 5.0, 8.0, 10.0, 20.0
Beam span l (m)	1.0, 1.5, 2.0, **2.5**, 3.0, 3.5, 4.0, 4.5, 5.0
Beam section (m × m)	0.1×0.2, 0.15×0.2, **0.15×0.25**, 0.15×0.3, 0.2×0.3, 0.2×0.4, 0.2×0.5, 0.25×0.5, 0.3×0.5
Rebar ratio at tensile side ρ (%)	0.42, 0.60, 0.82, **1.07**, 136, 1.68, 2.03, 2.51

A total of six key parameters affecting the impact force profile are employed in this analytical study as listed in Table 3. The values marked in red for each parameter are the reference value for the analytical parametric study, that is, in each case only one parameter is changed while other parameters adopt the reference values. Without loss of generality in this study, the values for the six parameters used to fit empirical equations are chosen from the widely used design parameters in drop weight impact tests as given in Table 3. A total of 59 specimens considering different combinations of parameters listed in Table 3 are investigated to obtain the impact force profile by using the calibrated 2DOF analytical method. Once the impact force profile of each specimen is generated from the analytical results, the characteristic points illustrated in Fig. 17 are determined and collated into a database. Through multivariable regression analysis, six empirical equations (22)~(27) are proposed to predict the impact force and duration of characteristic points by using the parameters with their own dimensions. It should be noted that the beam section flexural stiffness *EI* (10^6 N·m^2) is included in these equations to quantify the effect of the beam section on the global stiffness and plateau force. If the empirical equations (22)~(27) are used to predict the impact force profile, the six parameters should be chosen within the applicable range with the specified units as listed in Table 3

$$F_a = 302.02{k_\mathrm{c}}^{0.588} + 0.78{m_\mathrm{d}}^{0.5} + 62.88v_0 - 259.49 \qquad (R^2 = 0.94) \qquad (22)$$

$$F_\mathrm{p} = 19.97{k_\mathrm{c}}^{0.26} + 15.82{v_0}^{0.32} + 160.22l^{-0.9} + 47.25\ln(EI) + 41.18\rho - 185 \qquad (R^2 = 0.93) \qquad (23)$$

$$t_a = 0.84 + \frac{0.112}{k_c} + \frac{0.148}{v_0} \qquad (R^2 = 0.82) \qquad (24)$$

$$t_b = e^{(-0.08k_c + 0.0002m_d + 0.0046v_0 + 1.2)} \qquad (R^2 = 0.75) \qquad (25)$$

$$t_{cd} = e^{(0.00123m_d + 0.135v_0 + 0.348l - 0.047EI - 0.8\rho + 2.55)} \qquad (R^2 = 0.88) \qquad (26)$$

$$t_e = e^{(0.001m_d + 0.1v_0 + 0.307l - 0.036EI - 0.535\rho + 2.993)} \qquad (R^2 = 0.89) \qquad (27)$$

4.3. Verification of the simplified impact force profile model

To verify the proposed equations (22)~(27) for predicting the impact force and duration of the simplified impact force profile, a total of 39 sets of tested data including experimental results [22, 26, 52, 53] and numerical results in section 3.2 are used for validation. All the 39 sets of data have the Type III impact force profile and the failure models are global flexure or flexure-shear failure instead of severe local shear failure. Fig. 18 shows the comparison of the test data and predicted results of the characteristic points. The coefficient of correlation *R* between test data and predicted results and the mean value of predicted-to-tested ratio (Mean) are given. Fig. 18(a)~(b) show that the predicted impact forces (F_a and F_p) present good correlations with the test data by yielding R = 0.984 and Mean = 0.998 for the peak force, and R = 0.889 and Mean = 1.028 for the plateau force. Besides, the predicted durations as shown in Fig. 18(c)~(f) also agree well with the test data. It is noted that the coefficient of correlation R of the peak force time t_a and primary duration t_b are relatively lower than those of force plateau duration t_{cd} and total impact duration of t_e because the linear behaviour of the contact stiffness is employed in this analytical study.

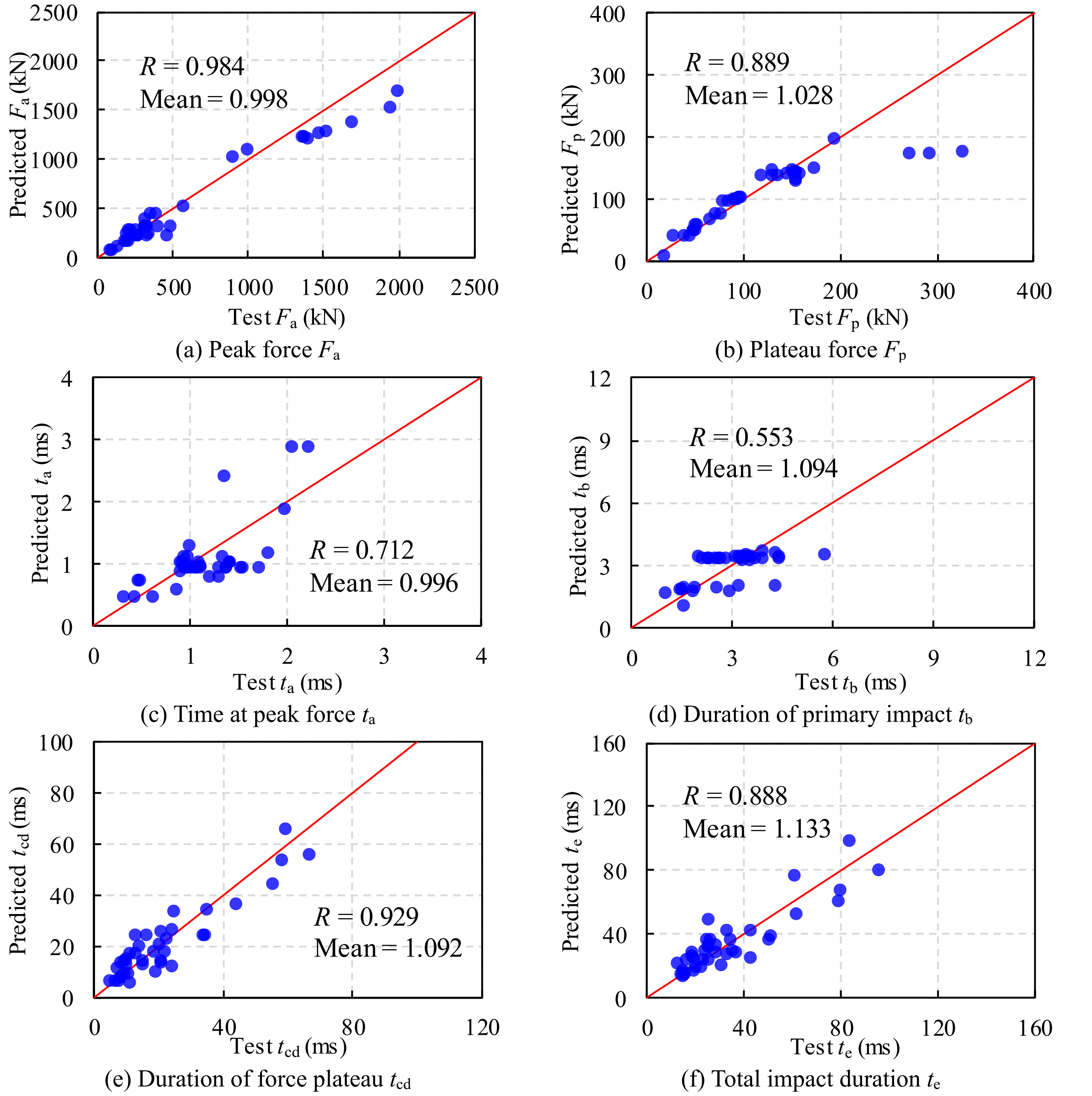

(a) Peak force F_a (b) Plateau force F_p

(c) Time at peak force t_a (d) Duration of primary impact t_b

(e) Duration of force plateau t_{cd} (f) Total impact duration t_e

Fig. 18. Comparison of test and predicted values for characteristic points.

Based on the impulse-momentum conservation theorem, the impulse is equal to the change of the momentum during impact. Upon drop weight impact, the beam at midspan reaches the maximum displacement and the velocities of beam and drop weight are zero at point *D* as shown in Fig 17. Therefore, the impulse calculated by the area of *OABCDF*, i.e., the grey area in Fig 17 should be equal to the initial momentum of drop weight. In order to further verify the proposed equations for impact force profile, the initial momentum of drop weight and predicted impulse are compared as shown in Fig. 19. The predicted impulse applied on the beam is comparable to the initial momentum of drop weight, with the correlation value R = 0.878 and Mean = 1.252.

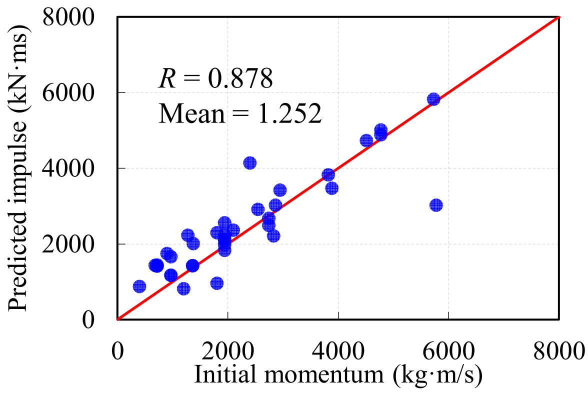

Fig. 19. Comparison of initial momentum and predicted impulse.

In addition, the simplified impact force profiles predicted by the proposed equations are also compared with experimental results as shown in Fig. 16(a). It is observed that the predicted simplified impact force profiles are in good agreement with the tested impact force profile in general. It is concluded that the proposed equations can well predict the simplified impact force profile for pin-supported RC beams under drop weight impact.

4.4. Discussion on the applicability of the proposed analytical model

The 2DOF analytical model for pin-supported RC beams under drop weight impact is developed and the empirical formulae for predicting the simplified impact force profile are also proposed based on test and analytical results. The proposed formulae give a good prediction of the overall impact force profile and can rapidly predict the simplified impact force profile for the design of drop weight impact tests. However, since only the global stiffness of RC beams is considered in the analytical derivation while the local shear stiffness of RC beams is ignored, the proposed simplified impact force profile model is only applicable for the RC beams with global flexure or flexure-shear deformation under impact. Therefore, the failure mode of RC beams under impact should be examined first to determine the applicability of the proposed models. Whether the beam experiencing shear failure depends on the characteristic of impact loading (duration and amplitude) and the impact load-carrying capacity of beam [54-57]. If the impact loading amplitude is high and the ratio of T_m/T_M is very small, the failure mode of beam is governed by shear or/and punching shear failure [54, 55]. In addition, the beam subjected to an impact loading with peak force higher than the dynamic shear load-capacity of beam section is prone to experience punching shear failure [56, 57]. Diagonal shear cracks occur along the failure section with an approximate angle of 45° [5, 8, 56] as shown in Fig. 20. Therefore, the failure mode of beam can be pre-determined by comparing the peak impact force and the dynamic shear capacity P_{dyn}^{max} of the beam section.

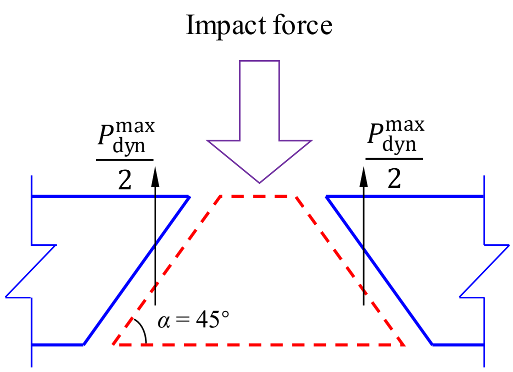

Fig. 20. Local punching shear failure of beam section.

The dynamic shear capacity $P_{\mathrm{dyn}}^{\max}$ of RC beams can be estimated by using the simplified equation proposed by Do et al. [57] as follows:

$$P_{\mathrm{dyn}}^{\max} = 6.5 \times \frac{f_c'}{10} \times b \times d \tag{28}$$

where b and d are the width and depth of beam section, f_c' is the concrete compressive strength. Local punching shear failure appears when the peak impact force reaches $P_{\mathrm{dyn}}^{\max}$. Therefore, to determine the failure mode of RC beam, the peak impact force can be firstly estimated by Eq. (22) and then compared with $P_{\mathrm{dyn}}^{\max}$. If the calculated peak impact force is less than the dynamic shear capacity $P_{\mathrm{dyn}}^{\max}$ of beam section, it is deemed that RC beam presents global deformations instead of severe local punching shear failure and the proposed equations (22)~(27) can be used to predict the impact force profile of RC beam.

5. Conclusion

The impact force profile of RC beams under drop weight impact is numerically and analytically investigated in this study. The factors affecting the impact force profile are summarized and the influence of the global stiffness on the impact force plateau is quantified. A 2DOF analytical model is developed to predict the impact force profile with good accuracy. The simplified impact force profile can be straightforwardly estimated by using empirical equations (22)~(27). The main conclusions can be drawn as follows.

1. The global stiffness governs the impact force plateau but has a negligible effect on the peak impact force. Decreasing the global stiffness of RC beam would weaken the interaction between the drop weight and the beam after the primary impulse, causing a decrease of

plateau force and an increase of plateau stage duration.

2. A 2DOF analytical model is developed for the pin-supported RC beams under drop weight impact, and gives accurate predictions of impact force and beam displacement response.
3. Intensive analytical calculations are carried out to predict the impact force profiles, and the results are used together with available testing data to develop empirical formulae for predictions of impact forces. The proposed empirical formulae are proven yielding good predictions of impact force profiles that would be induced by drop weight on RC beams.

Acknowledgements

The authors acknowledge the financial support from Australian Research Council (ARC) via Australian Laureate Fellowship (FL180100196). The first author also gratefully acknowledges the financial support from Curtin International Postgraduate Research Scholarship (CIPRS) and Curtin Strategic International Research Scholarship (CSIRS).

References

[1]. Hwang, H.-J., Yang, F., Zang, L., Baek, J.-W., and Ma, G., *Effect of Impact Load on Splice Length of Reinforcing Bars.* International Journal of Concrete Structures and Materials, 2020. 14(1): 40.

[2]. Teles, D.V.C., Oliveira, M.C., and Amorim, D.L.N.F., *A simplified lumped damage model for reinforced concrete beams under impact loads.* Engineering Structures, 2020. 205: 110070.

[3]. Kishi, N., Komuro, M., Kawarai, T., and Mikami, H., *Low-Velocity Impact Load Testing of RC Beams Strengthened in Flexure with Bonded FRP Sheets.* Journal of Composites for Construction, 2020. 24(5).

[4]. Zhao, D., Yi, W., and Kunnath, S.K., *Shear Mechanisms in Reinforced Concrete Beams under Impact Loading.* Journal of Structural Engineering, 2017. 143(9): 04017089.

[5]. Fu, Y., et al., *Investigating the failure behaviors of RC beams without stirrups under impact loading.* International Journal of Impact Engineering, 2020. 137: 103432.

[6]. Pham, T.M., Chen, W., Elchalakani, M., Karrech, A., and Hao, H., *Experimental investigation on lightweight rubberized concrete beams strengthened with BFRP sheets subjected to impact loads.* Engineering Structures, 2020. 205: 110095.

[7]. Li, H., Chen, W., and Hao, H., *Dynamic response of precast concrete beam with wet connection subjected to impact loads.* Engineering Structures, 2019. 191: 247-263.

[8]. Saatci, S. and Vecchio, F.J., *Effects of shear mechanisms on impact behavior of reinforced concrete beams.* ACI structural Journal, 2009. 106(1): 78-86.

[9]. Pham, T.M. and Hao, H., *Impact Behavior of FRP-Strengthened RC Beams without Stirrups.* Journal of Composites for Construction, 2016. 20(4): 04016011.

[10]. Li, H., Chen, W., and Hao, H., *Factors influencing impact force profile and measurement accuracy in drop weight impact tests.* International Journal of Impact Engineering, 2020. 145: 103688.

[11]. Tachibana, S., Masuya, H., and Nakamura, S., *Performance based design of reinforced concrete beams under impact.* Natural Hazards and Earth System Sciences, 2010. 10(6): 1069-1078.

[12]. Zhao, W., Qian, J., and Jia, P., *Peak Response Prediction for RC Beams under Impact Loading.* Shock and Vibration, 2019. 2019: 1-12.

[13]. Li, H., Chen, W., and Hao, H., *Influence of drop weight geometry and interlayer on impact behavior of RC beams.* International Journal of Impact Engineering, 2019. 131: 222-237.

[14]. Pham, T.M. and Hao, H., *Effect of the plastic hinge and boundary conditions on the impact behavior of reinforced concrete beams.* International Journal of Impact Engineering, 2017. 102: 74-85.

[15]. Adhikary, S.D., Li, B., and Fujikake, K., *Low Velocity Impact Response of Reinforced Concrete Beams: Experimental and Numerical Investigation.* International Journal of Protective Structures, 2015. 6(1): 81-111.

[16]. Pham, T.M. and Hao, H., *Prediction of the impact force on reinforced concrete beams from a drop weight.* Advances in Structural Engineering, 2016. 19(11): 1710-1722.

[17]. Hao, H., Hao, Y., Li, J., and Chen, W., *Review of the current practices in blast-resistant analysis and design of concrete structures.* Advances in Structural Engineering, 2016. 19(8): 1193-1223.

[18]. Yi, W., Zhao, D., and Kunnath, S.K., *Simplified approach for assessing shear resistance of reinforced concrete beams under impact loads.* ACI Structural Journal, 2016. 113(4): 747.

[19]. Zhou, X., Zhang, R., Xiong, R., Zhang, G., and Wang, X., *An Experimental Study of the Impact Mechanical Properties of RC Beams following Replacements of Stainless Steel Reinforcements of Equal Strength.* Advances in Materials Science and Engineering, 2019. 2019: 1-16.

[20]. Fan, W., Liu, B., Huang, X., and Sun, Y., *Efficient modeling of flexural and shear behaviors in reinforced concrete beams and columns subjected to low-velocity impact loading.* Engineering Structures, 2019. 195: 22-50.

[21]. Hwang, H.-J., Kang, T.H.K., and Kim, C.-S., *Numerical Model for Flexural Behavior of Reinforced Concrete Members Subjected to Low-Velocity Impact Loads.* ACI Structural

Journal, 2019. 116(2): 65-3.

[22]. Jin, L., Zhang, R., Dou, G., Xu, J., and Du, X., *Experimental and numerical study of reinforced concrete beams with steel fibers subjected to impact loading.* International Journal of Damage Mechanics, 2018. 27(7): 1058-1083.

[23]. Jiang, H., Wang, X., and He, S., *Numerical simulation of impact tests on reinforced concrete beams.* Materials & Design, 2012. 39: 111-120.

[24]. Bhatti, A.Q., Kishi, N., Konno, H., and Mikami, H., *Elasto-plastic dynamic response analysis of prototype RC girder under falling-weight impact loading considering mesh size effect.* Structure and Infrastructure Engineering, 2012. 8(9): 817-827.

[25]. Yoo, D.-Y., Banthia, N., Kim, S.-W., and Yoon, Y.-S., *Response of ultra-high-performance fiber-reinforced concrete beams with continuous steel reinforcement subjected to low-velocity impact loading.* Composite Structures, 2015. 126: 233-245.

[26]. Fujikake, K., Li, B., and Soeun, S., *Impact Response of Reinforced Concrete Beam and Its Analytical Evaluation.* Journal of Structural Engineering, 2009. 135(8): 938-950.

[27]. Chen, W., Hao, H., and Chen, S., *Numerical analysis of prestressed reinforced concrete beam subjected to blast loading.* Materials & Design, 2015. 65: 662-674.

[28]. Gholipour, G., Zhang, C., and Mousavi, A.A., *Loading rate effects on the responses of simply supported RC beams subjected to the combination of impact and blast loads.* Engineering Structures, 2019. 201: 109837.

[29]. Hao, Y. and Hao, H., *Influence of the concrete DIF model on the numerical predictions of RC wall responses to blast loadings.* Engineering Structures, 2014. 73: 24-38.

[30]. Malvar, L.J., *Review of static and dynamic properties of steel reinforcing bars.* Materials Journal, 1998. 95(5): 609-616.

[31]. Pham, T.M. and Hao, H., *Influence of global stiffness and equivalent model on prediction of impact response of RC beams.* International Journal of Impact Engineering, 2018. 113: 88-97.

[32]. Machado, M., Moreira, P., Flores, P., and Lankarani, H.M., *Compliant contact force models in multibody dynamics: Evolution of the Hertz contact theory.* Mechanism and Machine Theory, 2012. 53: 99-121.

[33]. Sun, J., Lam, N., Zhang, L., Ruan, D., and Gad, E., *A note on Hunt and Crossley model with generalized visco-elastic damping.* International Journal of Impact Engineering, 2018. 121: 151-156.

[34]. Wang, H., Yin, X., Hao, H., Chen, W., and Yu, B., *The correlation of theoretical contact models for normal elastic-plastic impacts.* International Journal of Solids and Structures, 2020. 182-183: 15-33.

[35]. Sun, J., Lam, N., Zhang, L., Ruan, D., and Gad, E., *Contact forces generated by hailstone impact.* International Journal of Impact Engineering, 2015. 84: 145-158.

[36]. Perera, S., et al., *Deterministic solutions for contact force generated by impact of windborne debris.* International Journal of Impact Engineering, 2016. 91: 126-141.

[37]. Zhao, D., Yi, W., and Kunnath, S.K., *Numerical simulation and shear resistance of reinforced concrete beams under impact.* Engineering Structures, 2018. 166: 387-401.

[38]. Pham, T.M., Hao, Y., and Hao, H., *Sensitivity of impact behaviour of RC beams to contact*

stiffness. International Journal of Impact Engineering, 2018. 112: 155-164.

[39]. Hallquist, J.O., *LS-DYNA theory manual.* Livermore software Technology corporation, 2006: 531.

[40]. Sun, J., Lam, N., Zhang, L., Gad, E., and Ruan, D., *Contact forces generated by fallen debris.* Structural Engineering and Mechanics, 2014. 50(5): 589-603.

[41]. Fujikake, K., Senga, T., Ueda, N., Ohno, T., and Katagiri, M., *Study on impact response of reactive powder concrete beam and its analytical model.* Journal of advanced concrete technology, 2006. 4(1): 99-108.

[42]. Anagnostopoulos, S.A., *Pounding of buildings in series during earthquakes.* Earthquake Engineering and Structural Dynamics, 1988. 16(3): 443-456.

[43]. Cotsovos, D.M., Stathopoulos, N.D., and Zeris, C.A., *Behavior of RC Beams Subjected to High Rates of Concentrated Loading.* Journal of Structural Engineering, 2008. 134(12): 1839-1851.

[44]. Wu, K.Q. and Yu, T.X., *Simple dynamic models of elastic–plastic structures under impact.* International Journal of Impact Engineering, 2001. 25(8): 735-754.

[45]. Kent, D.C. and Park, R., *Flexural members with confined concrete.* Journal of the Structural Division, 1971. 97: 1969-1990.

[46]. Scott, B.D., Park, R., and Priestley, M.J.N., *Stress-Strain Behavior of Concrete Confined by Overlapping Hoops at Low and High Strain Rates.* ACI Journal, 1982. 79(1): 13-27.

[47]. Mazzoni, S., Mckenna, F., Scott, M.H., and Fenves, G.L., *OpenSees command language manual*. 2006, Pacific Earthquake Engineering Research Center: California.

[48]. Shi, Y.-L., Li, H., Wang, W.-D., and Hou, C., *A Fiber Model Based on Secondary Development of ABAQUS for Elastic–Plastic Analysis.* International Journal of Steel Structures, 2018. 18(5): 1560-1576.

[49]. Esmaeily, A. and Xiao, Y., *Behavior of Reinforced Concrete Columns Under Variable Axial Loads: Analysis.* ACI Structural Journal, 2005. 102(5): 736-744.

[50]. Stochino, F. and Carta, G., *SDOF models for reinforced concrete beams under impulsive loads accounting for strain rate effects.* Nuclear Engineering and Design, 2014. 276: 74-86.

[51]. Mattock, A.H., *Discussion of "Rotation Capacity of Reinforced Concrete Beams".* Journal of the Structural Division, 1967. 93(2): 519-522.

[52]. Xu, B. and Zeng, X., *Experimental study on the behaviors of reinforced concrete beams under impact loadings.* China Civil Engineering Journal, 2014. 47(2): 41-51.

[53]. Chen, Y. and May, I.M., *Reinforced concrete members under drop-weight impacts.* Proceedings of the Institution of Civil Engineers-Structures and Buildings, 2009. 162(1): 45-56.

[54]. Yang, Y., Lam, N., and Zhang, L., *Estimation of response of plate structure subject to low velocity impact by a solid object.* International Journal of Structural Stability Dynamics, 2012. 12(06): 1250053.

[55]. Hao, H., *Predictions of Structural Response to Dynamic Loads of Different Loading Rates.* Journal of Protective Structures, 2015. 6(4): 585-605.

[56]. Zhao, W. and Qian, J., *Resistance mechanism and reliability analysis of reinforced*

concrete columns subjected to lateral impact. International Journal of Impact Engineering, 2020. 136: 103413.

[57]. Do, T.V., Pham, T.M., and Hao, H., *Impact force profile and failure classification of reinforced concrete bridge columns against vehicle impact.* Engineering Structures, 2019. 183: 443-458.